Supporting Information Text

SI Materials and Methods

Comparative modeling of the myosin-actin complex. RosettaCM (1) breaks up multiple templates to produce hybridized structures that contain information from different structures. Here we applied the RosettaCM scripts published in Ref (2). A detailed tutorial with examples can be found in the SI of this paper. The protocol involves three steps: 1. align the target sequence to templates with Clustal Omega (3) and prepare input files; 2. use the partial thread application to create threaded pdb files for each target-template alignment; 3. generate ensembles of models using the RosettaCM hybridize protocol, which includes three stages of assembly and optimization (1).

The final assembly consisted of one human β-cardiac myosin (MYH7) and two adjacent α-cardiac actin (ACTC1) monomers. For the PPS state modeling, PDBs 5N69 (PPS, bovine cardiac muscle) and 5H53 (rigor, rabbit skeletal muscle) were used as the templates. The cardiac myosin sequence was aligned to the two template sequences and the cardiac actin sequence was aligned to that of 5H53. After partial threading, the threaded pdb of 5N69 included all the atoms of the original pdb; the threaded pdb of 5H53 included the two actin monomers in contact with myosin, as well as the key myosin loop motifs at the interface. For the rigor state modeling, the myosin-actin complex in 5H53 was used as the template. For the ADP-bound modeling, the myosin-actin complex in 6C1D (myosin 1b) was used as the template. The PPS and ADP-bound states have ATP hydrolysis products bound at the active site, which were incorporated by adding the additional flags "-extra_res_fa" and "-extra_res_cen" in the RosettaCM command to load the full-atom and centroid mode ligand parameters. The Rosetta module molfile_to_params.py was used to generate the Pi ($H_2PO_4^-$) and ADP parameters.

MD simulation setup. The top 35 conformations from each ensemble (PPS, ADP-bound, and rigor states) were selected for the following MD simulations. All the systems were solvated in a TIP3P water box with 150 mM NaCl. All the MD simulations were performed using the GPU-accelerated version of Amber18 (4, 5) with the ff14SB force field (6). The phosphate ion was modeled as $H_2PO_4^-$, which is the protonation state proposed for the product state (7, 8). Antechamber and the general AMBER force field (GAFF2) (9, 10) were applied to assign bonded and LJ parameters for Pi, whose partial charges were assigned according to Ref (11). An existing set of ADP parameters (12) and a multisite Mg^{2+} model (13) were used. Amber's tleap program was employed to generate the input files.

Simulation protocol. For each MD system built on a Rosetta model, three independent replica runs were performed, as described below. Firstly energy minimization was carried out while constraining the protein positions with 1 kcal/(mol Å^2) harmonic constraints. With the same position constraints, a following 10 ns equilibration simulation was performed at 300 K. To maintain the temperature, Langevin dynamics with a friction coefficient of 1 ps^{-1} was applied. Particle Mesh Ewald (14) was used for full-system periodic electrostatics while a 9 Å cutoff was applied to Lennard-Jones interactions. Bonds involving hydrogen atoms were constrained using SHAKE algorithm (15). The initial simulations filtered out a few systems that resulted in unstable dynamics. We then ran a subsequent GaMD simulation (16) for each MD system that passed the equilibration stage.

GaMD accelerates the sampling of protein conformational transitions by reducing the energy barrier with a harmonic boost potential (16). It has been successful in studying a few molecular machines, such as GPCR (17), CRISPR-Cas9 (18), and γ-secretase (19). Here the GaMD module implemented in Amber (16) was employed to perform the simulations, which included a 10-ns conventional MD stage and a 25-ns GaMD stage in the isothermal-isobaric ensemble at 1 bar and 300 K. The 10-ns conventional MD was used to collect statistics for calculating GaMD acceleration parameters. In the GaMD stage, the total potential energy surface was smoothed by a boost potential that had a 6 kcal/mol upper limit of the standard deviation for accurate reweighting. MC barostat (20) was chosen for pressure control. The accumulated GaMD trajectories lasted 2.0 μs, 2.1 μs, and 2.6 μs for the pre-powerstroke, rigor, and ADP-bound states, respectively.

Data analyses. To obtain two-dimemsional (2D) free energy profiles from the GaMD runs, we construct a 2D histogram with a total number of M bins, which cover the 2D space of interest. We define $\delta_{m,i}$ as the indicator function (21) for the ith frame of the trajectory through

$$\delta_{m,i} = \begin{cases} = 1 & \text{if frame } i \text{ falls in bin } m \\ = 0 & \text{otherwise} \end{cases} \quad [1]$$

The weighted histogram at bin m can be computed by

$$H_m = \sum_{i=1}^{N} \delta_{m,i} e^{\beta \Delta V_i} \quad [2]$$

where ΔV_i is the boost potential at the ith frame, N is the total number of frames, and $\beta = (k_B T)^{-1}$. The Maclaurin series expansion method was used to approximate the exponential term $e^{\beta \Delta V_i}$ (21). One can then determine the 2D free energy profile via

$$F_m = -k_B T \log H_m + F_0 \quad [3]$$

where F_0 is arbitrary constant which is chosen here to set the minimum value in the free energy profile to zero.

Movies 1 and 2 were rendered with VMD (22).

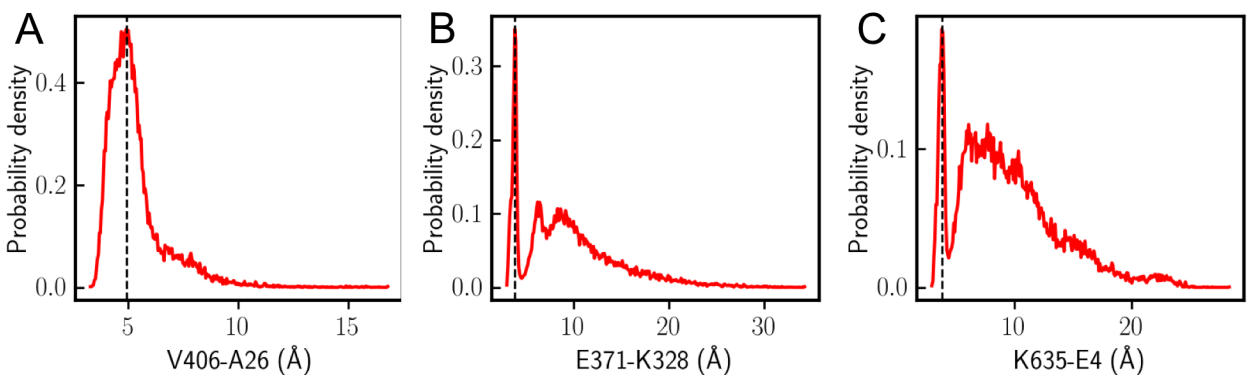

Fig. S1. Distance probability distributions of key residue pairs at the rigor state: A. the distance between the V406 and A26 (CB atoms); B. the distance between E371 (CD atom) and K328 (NZ atom); C. the distance between K635 (NZ atom) and E4 (CD atom, actin). The dashed black lines show the most probable distances.

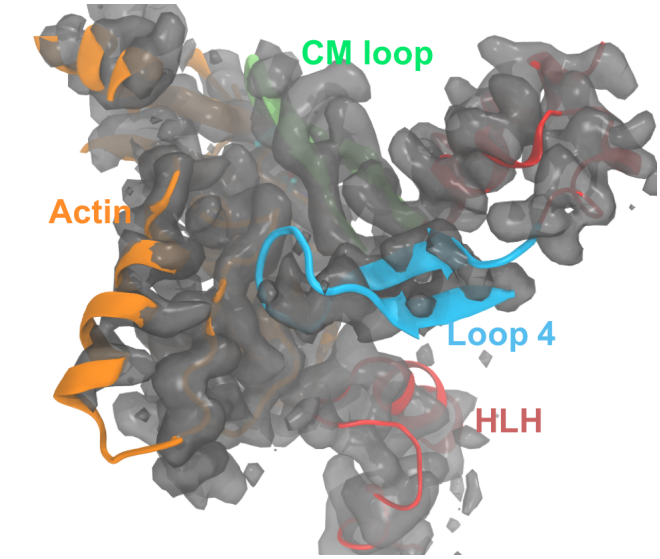

Fig. S2. Fitting key myosin-actin interface motifs into the cryo-EM density of rigor cardiac actomyosin (EMD-22335).

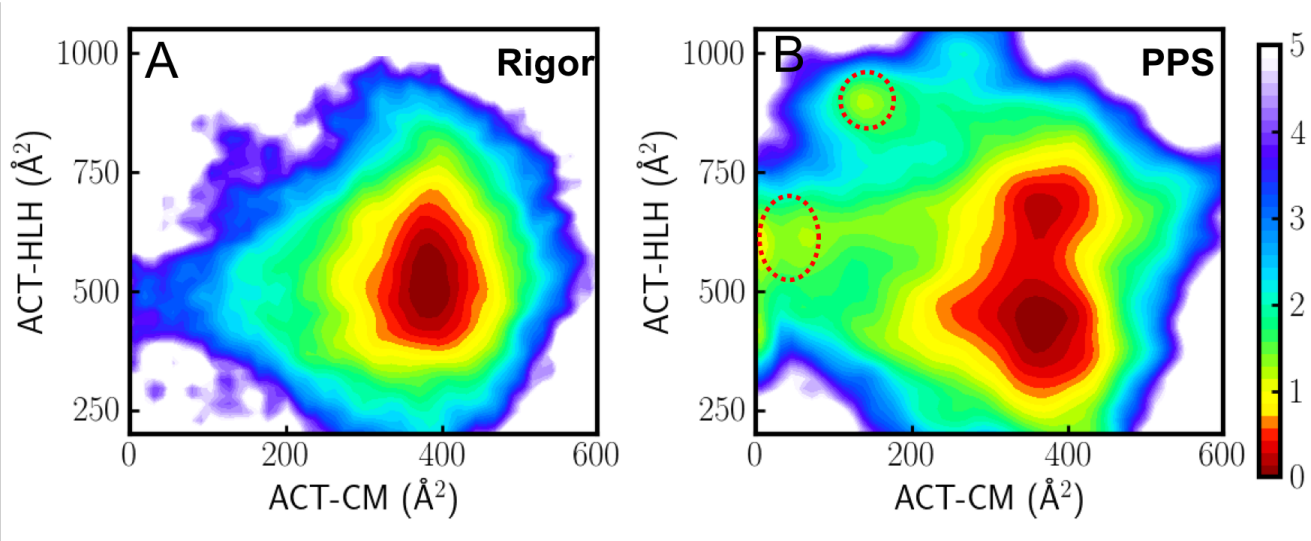

Fig. S3. 2D free energy profiles projected onto two contact area coordinates in the rigor (A) and PPS states (B). The contact area between actin and the CM loop (x-axis) is correlated with the contact area between actin and the HLH motif (y-axis). The red circles in the PPS landscape highlight two metastable states, in which the CM loop has relatively smaller contact areas with actin, while the HLH motif remains closely engaged with actin.

Movie S1. The actomyosin dynamics at the rigor state. loop 2, CM loop, loop 4, myosin motor domain, and actin are colored blue, lime, cyan, red and gray, respectively.

Movie S2. A gate is formed between switch I (yellow) and switch II (purple). P loop is colored green. Key residues (e.g. the gating residues R243 and E466) and Pi/ADP are shown in licorice representation.

References

1. Y Song, et al., High-resolution comparative modeling with rosettacm. *Structure* **21**, 1735–1742 (2013).
2. BJ Bender, et al., Protocols for Molecular Modeling with Rosetta3 and RosettaScripts. *Biochemistry* **55**, 4748–4763 (2016).
3. F Sievers, et al., Fast, scalable generation of high-quality protein multiple sequence alignments using clustal omega. *Mol. Syst. Biol.* **7**, 539 (2011).
4. D Case, et al., Amber 2018. *Univ. California, San Francisco* (2018).
5. R Salomon-Ferrer, DA Case, RC Walker, An overview of the amber biomolecular simulation package. *WIREs Comput. Mol. Sci.* **3**, 198–210 (2013).
6. JA Maier, et al., ff14SB: Improving the Accuracy of Protein Side Chain and Backbone Parameters from ff99SB. *J. Chem. Theory Comput.* **11**, 3696–3713 (2015).
7. FA Kiani, S Fischer, Catalytic strategy used by the myosin motor to hydrolyze atp. *Proc. Natl. Acad. Sci.* **111**, E2947–E2956 (2014).
8. ML Mugnai, D Thirumalai, Step-Wise Hydration of Magnesium by Four Water Molecules Precedes Phosphate Release in a Myosin Motor. *The J. Phys. Chem. B* **125**, 1107–1117 (2021).
9. J Wang, RM Wolf, JW Caldwell, PA Kollman, DA Case, Development and testing of a general amber force field. *J. Comput. Chem.* **25**, 1157–1174 (2004).
10. X He, VH Man, W Yang, TS Lee, J Wang, A fast and high-quality charge model for the next generation general AMBER force field. *The J. Chem. Phys.* **153**, 114502 (2020).
11. S Kashefolgheta, A Vila Verde, Developing force fields when experimental data is sparse: Amber/gaff-compatible parameters for inorganic and alkyl oxoanions. *Phys. Chem. Chem. Phys.* **19**, 20593–20607 (2017).
12. KL Meagher, LT Redman, HA Carlson, Development of polyphosphate parameters for use with the AMBER force field. *J. Comput. Chem.* **24**, 1016–1025 (2003).
13. A Saxena, D Sept, Multisite Ion Models That Improve Coordination and Free Energy Calculations in Molecular Dynamics Simulations. *J. Chem. Theory Comput.* **9**, 3538–3542 (2013).
14. T Darden, D York, L Pedersen, Particle mesh Ewald: An N?log(N) method for Ewald sums in large systems. *The J. Chem. Phys.* **98**, 10089–10092 (1993).
15. S Miyamoto, PA Kollman, Settle: An analytical version of the SHAKE and RATTLE algorithm for rigid water models. *J. Comput. Chem.* **13**, 952–962 (1992).
16. Y Miao, VA Feher, JA McCammon, Gaussian Accelerated Molecular Dynamics: Unconstrained Enhanced Sampling and Free Energy Calculation. *J. Chem. Theory Comput.* **11**, 3584–3595 (2015).
17. Y Miao, JA McCammon, Mechanism of the G-protein mimetic nanobody binding to a muscarinic G-protein-coupled receptor. *Proc. Natl. Acad. Sci.* **115**, 3036–3041 (2018).
18. G Palermo, Y Miao, RC Walker, M Jinek, JA McCammon, Crispr-cas9 conformational activation as elucidated from enhanced molecular simulations. *Proc. Natl. Acad. Sci.* **114**, 7260–7265 (2017).
19. A Bhattarai, et al., Mechanism of Tripeptide Trimming of Amyloid β-Peptide 49 by γ-Secretase. *J. Am. Chem. Soc.* **144**, 6215–6226 (2022).
20. J Åqvist, P Wennerström, M Nervall, S Bjelic, BO Brandsdal, Molecular dynamics simulations of water and biomolecules with a Monte Carlo constant pressure algorithm. *Chem. Phys. Lett.* **384**, 288–294 (2004).
21. LCT Pierce, R Salomon-Ferrer, C Augusto F. de Oliveira, JA McCammon, RC Walker, Routine Access to Millisecond Time Scale Events with Accelerated Molecular Dynamics. *J. Chem. Theory Comput.* **8**, 2997–3002 (2012).
22. W Humphrey, A Dalke, K Schulten, VMD – Visual Molecular Dynamics. *J. Mol. Graphics* **14**, 33–38 (1996).